OPTIMIZATION OF NSLS-II BLADE X-RAY BEAM POSITION MONITORS: FROM PHOTOEMISSION TYPE TO DIAMOND DETECTOR*

P. Ilinski#, Brookhaven National Laboratory, Upton NY, USA

Abstract

Optimization of blade type X-ray Beam Position Monitors (XBPM) was performed for NSLS-II undulator IVU20. Blade material, configuration and operation principle was analyzed to improve XBPM performance. Optimization is based on calculation of the XBPM signal spatial distribution. Along with standard photoemission blade XBPM, a Diamond Detector Blade (DDB) XBPM was analyzed. Analyses revealed, that Diamond Detector Blade XBPM would allow overcoming drawbacks of the photoemission type XBPMs.

INTRODUCTION

Photoemission blade XBPMs [1] are standard "white" beam XBPMs for most synchrotron radiation facilities. The photoemission XBPMs are non-invasive and can provide high spatial resolution, but they are vulnerable to the background radiation from dipoles and focusing optics due to their hypersensitivity to the lower energy photons. Performance of the photoemission type XBPM was analyzed to optimize geometry and configuration of photoemission blades. Optimization is based on calculations of the XBPM signal spatial distribution. An alternative type of a Diamond Detector Blade XBPM [2] was analyzed and compared to the photoemission XBPM.

UNDULATOR RADIATION SOURCE

Optimization of the XBPM was performed for the NSLS-II undulator IVU20. The power density spatial distribution at the minimum undulator gap, corresponding to K=1.8, and at 500 mA storage ring current is shown at Fig. 1.

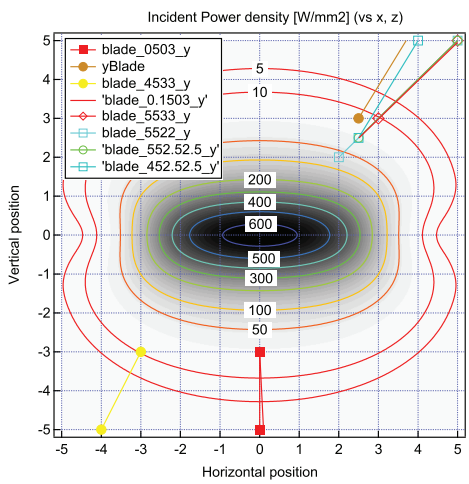

Figure 1: Power Density spatial distribution of undulator radiation [W/mm^2], IVU20, K=1.8, 10m.

The power density distribution specifies the high heat load conditions of the XBPM blades and defines how far away the blades should be placed from the axis of radiation, in order to withstand the heat load and to be mechanically stable since blade deformation can be interpreted as the undulator beam motion.

Another important characteristic for XBPM operation is the spectral flux angular dependence of the undulator radiation. The flux spectral density of IVU20 at various transverse locations from the axis of undulator radiation at 10m is presented in Fig. 2, it shows contribution of hard x-rays from high undulator harmonics at large off-axis angles.

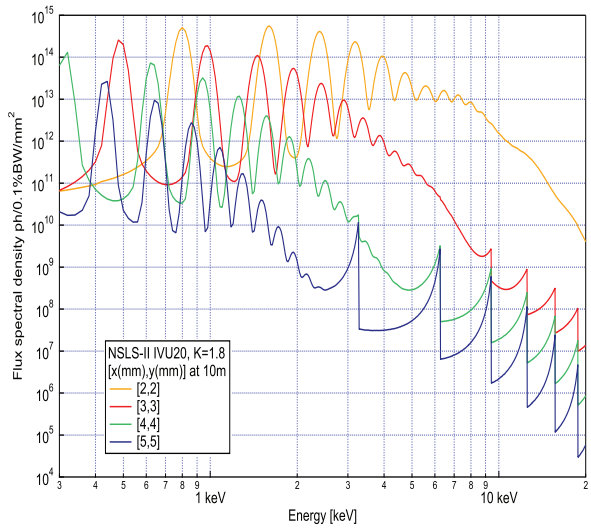

Figure 2: Flux Spectral Density angular dependance, IVU20, K=1.8, 10m at various transverse locations from the axis of radiation (x[mm], y[mm]).

PHOTOEMISSION BLADE XBPM

Operation of the photoemission XBPM is based on photoemission of electrons from a blade caused by x-rays. Tungsten is often used as a blade material for undulator XBPMs due to its mechanical properties. The resulting signal for photoemission XBPM is convolution of the undulator spectral density and the total electron yield of the blade material. The convolution for a portion of the undulator spectra will reveal signal distribution for particular undulator harmonic. The signal spatial distributions of tungsten blade are shown at Fig. 3 and Fig. 4 for the first and second undulator harmonics, respectively, for the IVU20, K=1.8, at 10m. The signal generated by second undulator harmonic is more intense and is localized closer to the axis of undulator radiation compare to the signal generated by the first undulator harmonic. The signal spatial distribution of tungsten blade which includes all undulator harmonics is presented at Fig. 5.

*Work supported by DOE contract DE-AC02-98CH10886
pilinski@bnl.gov

ISBN 978-3-95450-127-4

The signal level for various blade positions from Fig. 5 is reaching few hundreds of micro-amperes for 200-µm-thick tungsten blade at 10m distance for IVU20 at 500 mA current and K=1.8, reducing to tens of micro-amperes for K=0.5. The signal level will increase when blades are extended towards the axis of radiation, which however is limited due to the high heat load conditions.

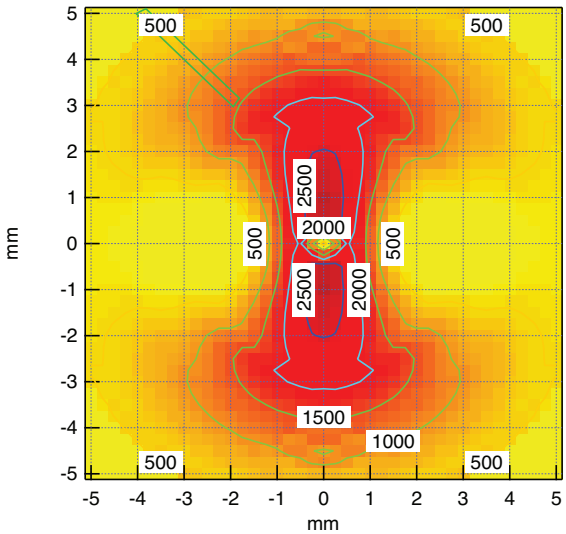

Figure 3: XBPM signal spatial distribution for tungsten blade [µA/mm^2], first undulator harmonic, IVU20, K=1.8, 10m.

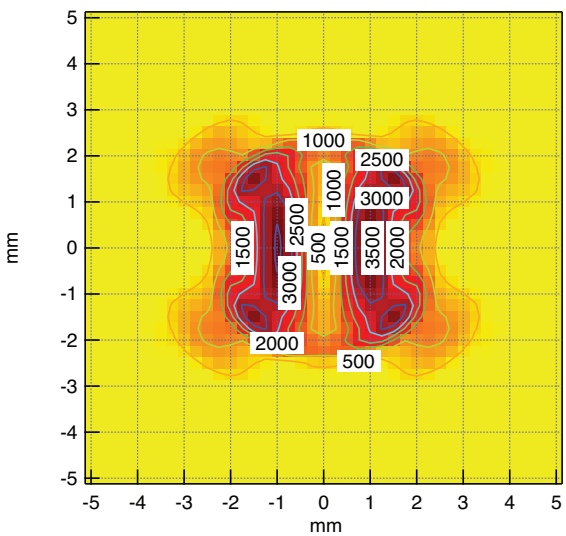

Figure 4: XBPM signal spatial distribution for tungsten blade [µA/mm^2], second undulator harmonic, IVU20, K=1.8, 10m.

Calibration curves, calculated as (S1-S2)/(S1+S2), where S1 and S2 are signals from the opposite blades for IVU20, K=1.8, 10m, are presented at Fig. 6 for different configurations of blades specified in Fig. 5. The sensitivity of the photoemission XBPM is characterized by the slope of the calibration curve. As can be seen, the calibration curves do not differ significantly when beam deviation is smaller then 0.5mm and therefore the sensitivity of the photoemission XBPM cannot be improved substantially by optimizing configuration of the blade which satisfies the high heat load conditions.

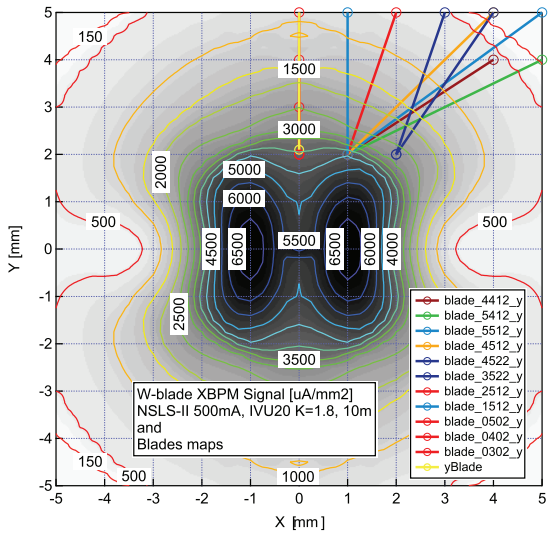

Figure 5: XBPM signal spatial distribution for tungsten blade [µA/mm^2], all undulator harmonics, IVU20, K=1.8, 10m.

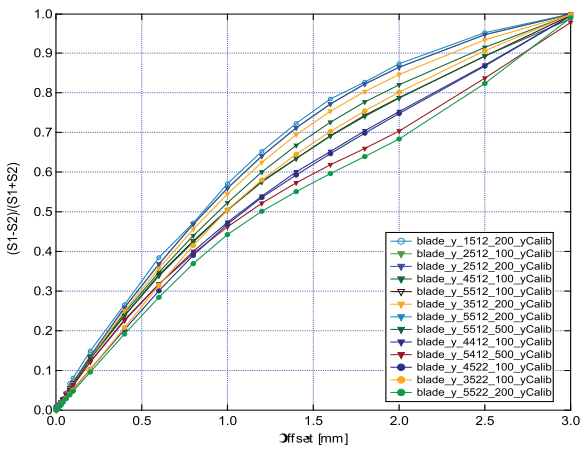

Figure 6: The calibration curves (S1-S2)/(S1+S2) of the tungsten blade XBPM for various blade configurations.

DIAMOND DETECTOR BLADE XBPM

Hypersensitivity to the lower energy photons and high dependence on the condition of the photoemission surface of the blade are major deficiencies of the photoemission type XBPM. Those deficiencies can be overcome by changing the photoemission blade to the Diamond Detector Blade. The DDB XBPM was introduced by H. Aoyagi [2], the layout of the DDB is shown at Fig. 7. The DDB is positioned along the radiation axis similar to the photoemission blade. Charge carriers, generated by photon absorbed in the diamond detector, drift to opposite side electrodes when bias voltage is applied. The signal generated in the diamond detector is proportional to the number and energy of absorbed photons through the conversion factor of ~13eV/e-h [3]. This proportionality

ISBN 978-3-95450-127-4

provides an intrinsic discrimination for the lower energy photons. Further discrimination can be achieved by not collecting charge carriers generated by low energy photons at the front of the DDB by offsetting the electrodes from the front edge of the DDB, Fig. 7. This is similar to an introduction of an x-ray filter in front of the DDB.

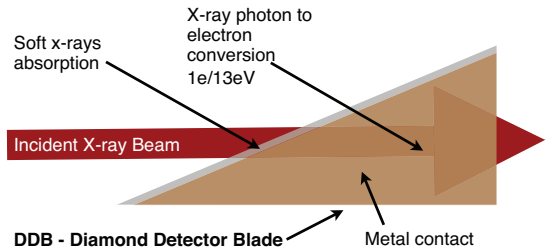

Figure 7: Layout of the diamond detector blade of the DDB XBPM.

The integrated spectral flux of undulator radiation from IVU20 at K=1.8 is shown at Fig. 8 along with the integrated spectral flux transmitted through 1-mm-thick and 16-mm-thick diamond filters. As can be seen, photons with energies below 4 keV will be fully absorbed in the 1-mm-thick diamond filter. Therefore, it will make possible to discriminate the lower energy photons and to control the DDB signal level by varying the thickness of the effective x-ray filter in front of the DDB. Further optimization of the side electrodes geometry can also allow control of important DDB characteristics such as capacitance.

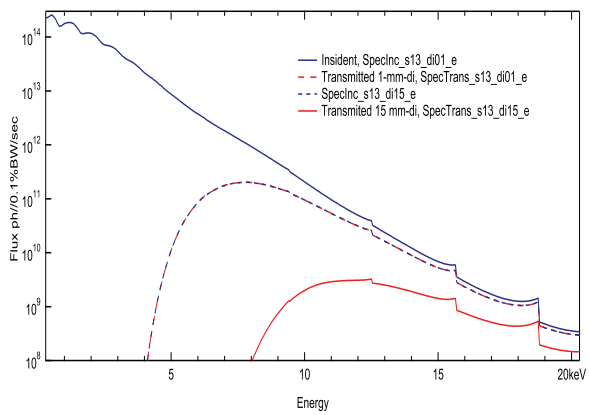

Figure 8: Integrated Spectral Flux of undulator radiation, IVU20, K=1.8 and incident undulator radiation transmitted through 1-mm-thick and 16-mm-thick diamond filters.

Because of ~13eV/e-h proportionality, the spatial distribution of the DDB XBPM signal reflects the spatial distribution of the incident radiation power density show at Fig.1. The DDB signal is reaching level of few hundreds of milli-amperes for IVU20, K=1.8, at 500 mA storage ring current. When a 1-mm-thick diamond x-ray filter is introduced in front of the DDB, the off-axis signal is attributed to the high undulator harmonics above 4 keV, as can be seen at Fig. 2. The signal spatial distribution becomes narrower, Fig. 9, the signal level drops to hundreds of micro-amperes. The calibration curves of the DDB XBPM with 1-mm-thick diamond x-ray filter in front of the DDB and without it are presented at Fig. 10 for various blade configurations. The sensitivity of the DDB XBPM without x-ray filter is two times higher compare to the tungsten blade XBPM form Fig. 6. The sensitivity of the DDB XBPM with x-ray filter depends on the blade position and is 6-8 times higher compare to the tungsten blade XBPM.

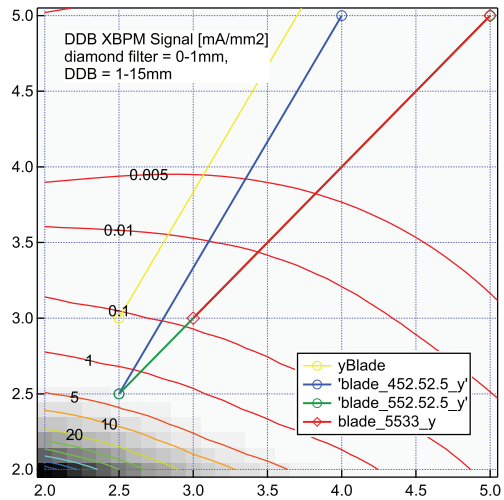

Figure 9: XBPM signal spatial distribution for Diamond Detector Blade [mA/mm^2], IVU20, K=1.8, 10m, 1-mm-thick diamond x-ray filter.

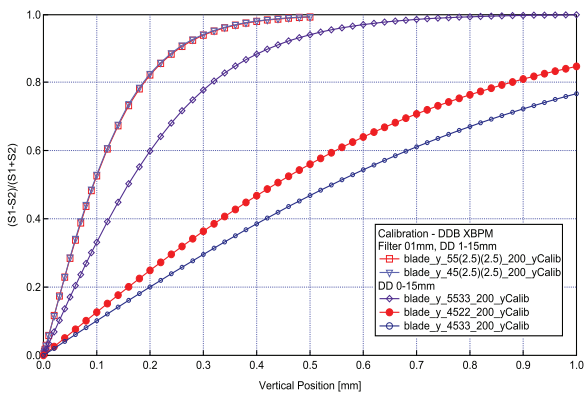

Figure 10: Calibration curves of the DDB XBPM for various blade configurations without and with 1-mm-thick diamond x-ray filter.

CONCLUSION

Analysis of the signal spatial distribution of the photoemission XBPM revealed that major contribution to the signal can be due to higher undulator harmonics. In particular case of the NSLS-II IVU20 at K=1.8 it is the second undulator harmonic, which mostly defines the signal level and the signal spatial distribution. The signal

ISBN 978-3-95450-127-4

level and the XBPM sensitivity can be increased by extending the blades towards the axis of radiation, which however is limited due to the high heat load conditions for blades. The photoemission XBPM sensitivity does not depend much on the configuration of the blades satisfying the high heat load conditions.

A novel type of the Diamond Detector Blade XBPM was analyzed as noninvasive "white" beam XBPM and compared to the photoemission XBPM. The choice of the Diamond Detector Blade instead of the photoemission blade as the source of the XBPM signal allows discrimination of the lower energy photons, which may have background origin. The discrimination is achieved due to proportionality of the DDB signal to the energy of absorbed x-ray photon and also by possible x-ray filtering through modification of the DDB side electrodes.

REFERENCES

[1] E.D. Johnson and T. Oversluizen, "Compact flux beam position monitor," Rev. Sci. Instrum. 60 (1989) 1947

[2] H. Aoyagi, T. Kudo, H. Tanida, and H. Kitamura, "New configuration of photoconductive type diamond detector head for x-ray beam position monitors," AIP Conf. Proc. 705 (2004) 933

[3] M. Pomorski et al., "Characterization of single crystal CVD diamond particle detectors for hadron physics experiments," Phys. Stat. Sol. (a) 202 (2005) 2199

ISBN 978-3-95450-127-4